Effect of prior oxidation on high cycle fatigue performance of RR1000 and role of oxidation in fatigue crack initiation

Cruchley, S.; Taylor, Mary; Li, Hangyue; Evans, H. E.; Bowen, P.; Child, D. J.; Hardy, M. C.

DOI:
10.1179/0960340914Z.00000000064

This is the Author's copy of an Accepted Manuscript of an article published by Taylor & Francis in Materials at High Temperatures on 19th January 2015, available online: http://www.tandfonline.com/doi/full/10.1179/0960340914Z.00000000064

Effect of Prior Oxidation on High Cycle Fatigue Performance of RR1000 and the Role of Oxidation in Fatigue Crack Initiation

S. Cruchley[1], M.P. Taylor[1], H.Y. Li[1], H.E. Evans[1], P. Bowen[1], D.J. Child[2] and M.C. Hardy[2]

[1]School of Metallurgy and Materials, University of Birmingham, Birmingham, B15 2TT, UK

[2]Rolls-Royce plc, Derby, DE24 8BJ, UK

Keywords: Oxidation, Fatigue crack initiation, High cycle fatigue

Abstract

The effect of prior oxidation on the room temperature fatigue life of coarse grained Ni-based superalloy, RR1000 has been performed at an R ratio of 0.1 with two pre-oxidation times: 100 and 2000 hours at 700°C. These pre-exposures produce extensive oxidation damage. The room temperature high cycle fatigue life of the pre-oxidised specimens has been compared to as-received specimens. At a maximum applied stress of 800 MPa a significant fatigue-life deficit is observed in the pre-oxidised testpieces. This is accompanied with the observations of significant cracking of the external chromia scale and the intergranular internal oxides within the area of maximum stress. Preferential cracking of oxides may lead to early crack initiation and consequently a reduction in total fatigue life.

Introduction

High temperature oxidation resistance is becoming increasingly important in Ni-based superalloys used in rotor disc applications since engine manufactures are under a significant amount of market pressure to improve fuel efficiency and reduce harmful emissions. This necessitates an increase in the rotor disc operating temperatures (~700°C), which will consequently result in increased environmental degradation. When these alloys oxidise they form a protective chromia external oxide scale along with significant internal oxidation of aluminium.[1-9] The internal oxides often form both intergranularly and intragranularly and are

preceded by a weaker region depleted in γ′ precipitates.[4-6] The role of environmental degradation in the mechanical performance of a component is important, since the formation of internal oxides is undesirable and may have a significant detrimental effect on the alloy.[10, 11] It has been postulated that internal oxides that form at alloy grain boundaries have the potential to act as preferential crack initiation sites [10] and therefore reduce component lives. This is especially the case when strengthening elements are removed during the formation of internal oxides.[10]

The effect of in-service environmental damage on component life can be investigated using extensive prior high temperature exposures. The effect of these exposures on the Ni-based superalloy, ME3, has shown that prior high temperature exposure to air (>700°C) for prolonged periods of times (100-2020h) has a detrimental effect on the high temperature (704°C) notched fatigue life. The reduction in fatigue life was found to be proportional to oxidation damage, with the thicker the external scale and deeper the internal damage the more pronounced the reduction in life.[8] The reduction in life was driven by $M_{23}C_6$ carbide dissolution as the removal of the internally oxidised region did not lead to a complete recovery in fatigue life whereas the removal of the carbide dissolution zone did. Another study using similar prior exposures on ME3 and Udimet 720 found that the mean lives of pre-exposed specimens had up to a 70% reduction in life, as well as a change in crack initiation location from sub-surface (as-received) to surface (pre-oxidised). Interestingly performing the prior exposures in vacuum led to no reduction in fatigue life illustrating that oxidation damage is driving the reduction in life.[12] Fatigue testing of IN100 in an oxidative environment has been shown to drastically reduce the time to crack initiation compared with tests performed in vacuum. The crack initiation life was similar to the number of cycles it took to fracture the oxide scale.[13] Pre-oxidation under an applied stress caused a further reduction in low cycle fatigue life in Rene 80 over both as-heat treated and unstressed pre-oxidised specimens.[14]

Oxides are inherently brittle structures with tensile failure strains of <1% and K_{1c} values for chromia and alumina in the range 0.4 - 2 $MPa.m^{1/2}$. These are typically much lower than the underlying metallic component, so it should be of no surprise that it is possible for these oxides to fail under tensile loading.[15] It is thought that the oxide intrusion ahead of the crack tip is susceptible to fracture leading to crack advancement.[13, 16-19] The aim of this present

study was to examine the potential for the intergranular internal oxides to act as preferential crack initiation sites and therefore affect the overall life of a component.

Experimental Method

Material

An advanced powder metallurgy Ni-based superalloy, RR1000 was adopted for this study. The alloy had received a solution heat treatment above the γ′ solvus and an aging treatment at 760ºC. This resulted in a coarse grain microstructure with most of the grains in the range of 30 to 50 μm and a bimodal distribution of secondary and tertiary γ′ particles (nominally Ni_3[Al, Ti]). The nominal composition of the alloy is in Table I.

Fatigue testing sample preparation

High cycle fatigue testing was performed on both as-received and pre-oxidised four-point bend specimens. The dimensions of the specimens were 100 mm x 9 mm x 10 mm. Specimens for pre-oxidation were ground and polished to a 6 μm (Ra =0.3 μm) finish and all edges and corners were chamfered to reduce stress concentrators and polished to the same surface finish. Specimens were cleaned and degreased in ethanol ultrasonically for a period of 5 minutes. They were then placed on top of two open ceramic alumina boats before being placed into a pre-heated Elite Thermal Systems Ltd. box furnace at 700°C for two time periods, either 2000 hours or 100 hours, in laboratory air. The furnace was previously calibrated using an N-type thermocouple to ±5°C. The furnace typically cooled by ~50°C on opening but regained the required temperature of 700°C within 10 minutes. In the non-oxidised condition the corners were chamfered to remove the potential for corner crack initiation and cleaned and degreased in ethanol ultrasonically for a period of 5 minutes. Otherwise the specimens were left as-received with the machining marks perpendicular to the direction of applied force.

High cycle fatigue testing

High cycle fatigue testing was performed on both as-received and pre-oxidised specimens at room temperature using an Amsler Vibrophore HCF machine, with a 20 kN load cell. A four point loading configuration with a span ratio of 60:20 mm was applied to all testpieces and testing was performed using an R ratio of 0.1. The load cells and cycle counters are calibrated yearly to ensure accurate application and measurement. The alignment of the

testing fixtures was checked before each test as any misalignment could induce unknown bending loads on the test specimens. Cycling was performed at the resonant frequency of the specimen, ~75 cycles per second. Testing was performed with a maximum applied stress of between 700 – 800 MPa at room temperature and is detailed in Table II. An oscilloscope was used to check and adjust the accuracy of the load applied. A test was stopped and defined a runout if it had not failed after $5x10^8$ cycles.

Sample preparation for SEM analysis

Failed fatigue specimens were treated with care to make sure the fracture surfaces remained free from contamination and were imaged using a Phillips XL-30 scanning electron microscope (SEM). The four-point bend specimens were prepared for detailed cross-section analysis by destructive examination. Specimens were mounted whole under vacuum in a low shrinkage, low viscosity epoxy resin. The region of highest stress was then cut out using a precision cutting machine at a low cutting speed (<0.05 mm/min) before being re-mounted in a low shrinkage, low viscosity epoxy resin. Samples were ground using progressively finer grades of wet SiC papers before being polished with progressively finer diamond solutions with final polishing being performed using OP-S colloidal silica solution. Specimens were cleaned ultrasonically with ethanol before being sputtered with gold for 60-120 seconds to allow SEM examination using a Jeol 7000F field emission gun (FEG) SEM. Etching was performed by swabbing the sample for 30 seconds using Kallings reagent (100 ml 96% ethanol, 100 ml 32% hydrochloric acid, 5g copper (II) chloride).

Focussed ion beam (FIB) analysis

FIB sectioning followed by secondary electron imaging was used to mill and analyse trenches through surface breaking cracks on failed four-point bend specimens to examine the nature of the near surface microstructure and the architecture of the cracks. This was performed using a Quanta 3D dual beam FEG FIB, with a 30 KeV gallium ion source. A protective tungsten layer (~35 x 3 x 4 μm) was deposited on top of the area of interest to protect from unwanted sputter damage. A beam current of 65 nA was used to mill an initial trench of dimensions 25 μm × 10 μm × 3 μm at 90° to the surface. Successively finer beam currents (30, 7, 1 and 0.5 nA) were used to polish the desired trench wall. This produced a clean smooth cross-section, which was imaged using the FEG electron beam in secondary electron mode.

Results and Discussion

The typical oxide morphology of the pre-oxidised specimens is shown in the cross-section of Figure 1. It can be seen that a continuous external oxide scale has formed on the surface with extensive sub-surface internal oxidation. This internal oxide occurs in two distinct locations in this alloy: intergranular and intragranular. The intergranular penetrations are deeper and often continuous whereas the intragranular penetrations consist of smaller isolated particles within the grains.[20] Elemental dispersive x-ray (EDX) analysis preformed in previous studies on this alloy have shown that the oxide composition of the external oxide scale is predominantly chromia with some isolated grains of rutile on the surface, and an alumina internal oxide.[3-6] This is typical of Ni-based superalloys used in rotor disc applications.[1, 7, 8, 21] The alumina penetrations draw aluminium out of the γ′ precipitates (Ni_3Al) causing a γ′ denuded zone to form ahead of the internally oxidised zone, this again penetrates into the alloy in two distinct penetrations (intergranular/intragranular) mirroring the internal oxide.[5, 20] Previous studies on Udimet 720, ME3 and RR1000 have found that oxidation under cyclic fatigue or dwell fatigue conditions leads to an enhancement in the oxidation damage but the composition of the oxide was consistent with the un-stressed pre-exposed condition.[12, 22] Therefore using pre-oxidation as a method of isolating the effect of environmental damage on fatigue performance is a reasonable approach.

Figure 2 clearly shows a high cycle fatigue deficit from the pre-oxidation of both 2000h and 100h at 700°C, with the pre-oxidised specimens showing 1-2 orders of magnitude reduction in life at a maximum outer fibre stress of 800 MPa. A further reduction in life is seen between the two pre-oxidation conditions, with the longer prior-exposure, and therefore increased depth of oxidation damage, causing a larger reduction in life. This suggests that the environmental damage is the cause of the reduction in life. A threshold for failure seems to occur at approximately 800 MPa, as at a peak stress of 700 MPa all testpieces runout at $5x10^8$ cycles and even at 800 MPa, failure is not guaranteed in the as-received condition, as a runout was recorded.

The initiation location of the as-received specimen and pre-oxidised specimens are compared in Figure 3. At room temperature and in the high cycle fatigue regime, it is generally observed that slip bands tend to form in the larger grains and lead to the initiation of fatigue cracks, although the contribution of neighbouring grains, by having nearly-similar Schmid factors, cannot be disregarded.[23] It is not surprising that the initiation site observed in the

current study was beneath the surface for the as-received specimens, as the large grains are distributed randomly and may not appear exactly on the top surface. It is also unlikely for the crack to initiate a long distance below the top surface as the stress level will be reduced significantly. Around the initiation site, fatigue crack growth demonstrates a faceted manner, which dictates the characteristics of the near threshold crack growth in which only limited slip systems are activated due to a small plastic zone. With further crack extension, such faceted crystallographic appearance is replaced with flat transgranular growth, which is typical for crack growth at higher stress intensity factor ranges, Paris regime. It is understood that the majority of total fatigue life is spent on initiating fatigue cracks for such smooth and small laboratory testpieces.

The fatigue crack initiation sites of the pre-oxidised specimens occurred at the surface in all cases of specimen failure (Figure 3). This indicates that the oxides are the source of crack initiation, although this is not conclusive because in four-point bend testing the surface regions experience the highest stress and therefore initiation would be expected. Other studies using cylindrical test specimens, where the surface region is not the region of highest stress, have similarly found surface initiations, however, with pre-oxidised specimens whereas sub-surface initiation occurred in the with as-received condition[12]. The present observations are consistent with these and add support to the notion that oxidation damage is the source of fatigue crack initiation.

A number of surface breaking cracks were seen near the fracture surfaces on the area of maximum tensile stress. A schematic diagram of the location of these cracks is shown in Figure 4. These cracks have been seen in both the pre-oxidised conditions (Figure 5a) but not in the as-received specimens. Additionally no cracking of the external oxide was seen in the un-failed pre-oxidised samples (700 MPa).

The reason for sectioning these surface breaking cracks is that they provide insight into the initiation process and how the main crack that caused failure initiated. In order to indicate whether these cracks originate from sub-surface environmental damage features, such as internal oxides, one was sectioned using focused ion beam microscopy. Figure 5 clearly shows the surface breaking crack cutting through the external chromia scale, penetrating down an intergranular internal oxide and proceeding into the alloy. Apart from the inevitable surface initiation the morphology is very similar. This is not unexpected since the surface

region is the area of highest tensile stress and these internal oxides are inherently sharp brittle structures with low fracture toughness forming along grain boundaries. The tensile failure strains (<1%) and fracture toughness of both chromia (K_{1c} ~ 2.0 MPa.m$^{1/2}$)[15] and alumina (K_{1c} ~ 0.4-1.0 MPa.m$^{1/2}$)[15] are significantly lower than the bulk alloy for which the fatigue crack growth threshold is around 10 MPa.m$^{1/2}$. It is therefore feasible that these oxides crack preferentially leading to early fatigue crack initiation and therefore a deficit in fatigue life, since initiation is known to constitute the majority of fatigue life.

This is supported by a previous study which found that surface oxide cracking and crack initiation is closely correlated[13]. It is also feasible in principle that the intergranular internal oxides are the source of initial cracking since alumina seems to have a lower fracture toughness than chromia and forms in an acicular morphology down the grain boundaries. Additionally, surface breaking cracks were only recorded in regions where there were significant intergranular oxides sub-surface. No surface breaking cracks were associated with intragranular internal oxides and no cracking of the intragranular internal oxides was seen. It could be the case that cracking of the intergranular internal oxide leads to a crack forming in both the external chromia scale and the sub-surface γ/γ′ alloy. Sudbrack et al (2012) found that the carbide dissolution zone was the main cause of the high temperature fatigue life deficit in the Ni-based superalloy, ME3, where weakened grain boundaries were thought to be the cause of initiation at high temperature[8]. In the present case, the carbide dissolution zone is present appreciably beyond the crack and internal oxides (Figure 6 & Table III) and therefore seems to have little effect on fatigue crack initiation. The crack visible in Figure 6 is fully contained within the oxides and has not propagated into the particle-free zone. Although these carbide-free grain boundaries could provide a weak path for the crack to propagate once it has initiated equally they may also inhibit crack growth as a result of stress relaxation. Additional work is on-going to try and provide further clarification.

Conclusion

- Room temperature four-point bend fatigue tests on RR1000 with and without pre-oxidation of up to 2000 hours at 700ºC were performed. A clear fatigue life deficit was found at a maximum stress of 800 MPa. A 1-2 orders of magnitude reduction in total fatigue life was found for the 2000 hour pre-oxidised condition and is attributed to a short initiation period.

- A change in initiation location from that in unoxidised specimens was seen after pre-oxidation, from sub-surface to surface locations. This indicated that oxidation damage, and not crystallographic facets, was the cause of early crack nucleation.
- Cracking of both the external chromia scale and the intergranular alumina internal precipitate can be seen in the pre-oxidised conditions at 800 MPa, with cracking of the external scale occurring above cracks in the intergranular oxides. It is therefore feasible that the intergranular internal oxides are the source of the fatigue crack initiation and therefore the fatigue life deficit.

Acknowledgements

The authors acknowledge, with thanks, the assistance provided by Jifeng Sun in producing the FIB sections. SC is grateful for financial support provided by the Engineering and Physical Sciences Research Council (EPSRC) and Rolls-Royce plc.

References

1. J. Chen, P. Rogers, and J. A. Little, *Oxidation of Metals*, 1997, **47**(5), 381-410.

2. D. Kim, C. Jang, and W. Ryu, *Oxidation of Metals*, 2009, **71**(5), 271-293.

3. A. Encinas-Oropesa, N. J. Simms, J. R. Nicholls, G. L. Drew, J. Leggett, and M. C. Hardy, *Materials at High Temperatures*, 2009, **26**(3), 241-249.

4. M. P. Taylor, H. E. Evans, S. Stekovic, and M. C. Hardy, *Materials at High Temperatures*, 2012, **29**(2), 145-150.

5. S. Cruchley, M. P. Taylor, H. E. Evans, P. Bowen, M. C. Hardy, and S. Stekovic: 'Microstructural Characterisation of High Temperature Oxidation of Nickel Base Superalloy RR1000 and the Effect of Shot-Peening', Superalloys 2012: 12th International Symposium on Superalloys, Seven Springs, PA, 2012, TMS, 751-758.

6. S. Cruchley, H. E. Evans, M. P. Taylor, M. C. Hardy, and S. Stekovic, *Corrosion Science*, 2013, **75**, 58-66.

7. G. A. Greene and C. C. Finfrock, *Oxidation of Metals*, 2001, **55**(5), 505-521.

8. C. K. Sudbrack, S. L. Draper, T. T. Gorman, J. Telesman, T. P. Gabb, and D. R. Hull: 'Oxidation and the Effects of High Temperature Exposures on Notched Fatigue Life of an Advanced Powder Metallurgy Disk Superalloy', Superalloys 2012: 12th International Symposium on Superalloys, Seven Springs, PA, 2012, TMS, 863-872.

9. K. Al-Hatab, M. Al-Bukhaiti, U. Krupp, and M. Kantehm, *Oxidation of Metals*, 2011, **75**(3), 209-228.

10. F. H. Stott and G. C. Wood, *Materials Science and Technology*, 1988, **4**, 1072-1078.

11. R. A. Rapp, *Corrosion* 1965, **21**(12), 382-401.

12. T. P. Gabb, J. Telesman, P. T. Kantzos, J. W. Smith, and P. F. Browning: 'Effects of high temperature exposures on fatigue life of disk superalloys', Superalloys 2004: 10th international symposium on superalloys, Seven Springs, PA, 2004, TMS, 269-274.

13. M. Reger and L. Remy, *Metallurgical Transactions A - Physical Metallurgy and Materials Science*, 1988, **19**(9), 2259-2268.

14. S. Antolovich, P. Domas, and J. L. Strudel, *Metallurgical Transactions A - Physical Metallurgy and Materials Science*, 1979, **10**(12), 1859-1868.

15. H. E. Evans, *International Materials Reviews*, 1995, **40**(1), 1-40.

16. E. Andrieu, R. Molins, H. Ghonem, and A. Pineau, *Materials Science and Engineering: A*, 1992, **154**(1), 21-28.

17. H. S. Kitaguchi, H. Y. Li, H. E. Evans, R. G. Ding, I. P. Jones, G. Baxter, and P. Bowen, *Acta Materialia*, 2013, **61**(6), 1968-1981.

18. H. E. Evans, H. Y. Li, and P. Bowen, *Scripta Materialia*, 2013, **69**(2), 179-182.

19. H. W. Liu and Y. Oshida, *Theoretical and Applied Fracture Mechanics*, 1986, **6**(2), 85-94.

20. S. Cruchley, M. P. Taylor, H. E. Evans, D. J. Child, and M. C. Hardy, *Materials Science and Technology - Accepted in Press*, 2014.

21. J. L. Evans, *Journal of Materials Engineering and Performance*, 2010, **19**(7), 1001-1004.

22. A. Karabela, L. G. Zhao, J. Tong, N. J. Simms, J. R. Nicholls, and M. C. Hardy, *Materials Science and Engineering: A*, 2011, **528**(19-20).

23. K. Kobayashi, K. Yamaguchi, M. Hayakawa, and M. Kimura, *International Journal of Fatigue*, 2008, **30**(10–11), 1978-1984.

Table Captions

Table I: Nominal composition of RR1000 in atomic and weight %.

Table II: High cycle fatigue testing matrix, all tests performed at room temperature.

Table III: Oxidation damage measurements, in microns, of both pre-oxidation conditions, 700°C for 100 and 2000 hours (± 1 standard deviation). Units in microns.

Figure Captions

Figure 1: BSE image of the cross-section through the typical oxidation damage produced by high temperature exposures at 700°C for a) 2000 hours and b) 100 hours at different magnifications.

Figure 2: A graph depicting the three conditions (as-received, 100h pre-oxidation and 2000h pre-oxidation) tested showing maximum applied stress against number of cycles to failure. An arrow underneath the symbol demonstrates a runout test at 5 $x10^8$ cycles.

Figure 3: Secondary electron images of the fracture surfaces of a) a pre-oxidised (2000h) specimen that failed after 610,000 cycles at 800 MPa. b) A pre-oxidised (100h) specimen that failed after 3.9 million cycles at 800 MPa. c) An as-received specimen that failed after 10.6 million cycles at 800 MPa. An arrow on each image indicates the crack initiation point.

Figure 4: Schematic diagram of a fractured four-point bend specimen illustrating the location of any surface breaking cracks that were subsequently sectioned. Maximum tensile stress is experienced on the bottom surface between the two wider rollers.

Figure 5: SE images taken using the electron beam on the FIB section of a pre-oxidised (2000h) specimen that failed after 610,000 cycles at 800 MPa with, a) surface breaking cracks in the external oxide and, b) section through surface breaking crack showing a crack progressing through the external oxide and intergranular internal oxide before progressing into the base alloy.

Figure 6: BSE image of an etched pre-oxidised (2000 hours) specimen that failed after 1.9 million cycles at a maximum applied stress of 800 MPa, showing cracking of external and intergranular internal oxides along with the presence of both a γ' denuded zone and carbide dissolution zone.

Table I

	Ni	Co	Cr	Mo	Ti	Al	Ta	Hf	Zr	C	B
Weight %	Bal	18.5	15.0	5.0	3.6	3.0	2.0	0.5	0.06	0.02	0.03
Atomic %	Bal	17.9	16.5	3.0	4.3	6.35	0.63	0.16	0.04	0.14	0.10

Table II

	Pre-oxidation	R Ratio	Stress [MPa]		
			σ_{min}	σ_{max}	σ_{mean}
1	2000h	0.1	70	700.0	385
2	2000h	0.1	80	800.0	440
3	2000h	0.1	80	800.0	440
4	2000h	0.1	80	800.0	440
5	2000h	0.1	80	800.0	440
6	No	0.1	70	700.0	385
7	No	0.1	80	800.0	440
8	No	0.1	80	800.0	440
9	100h	0.1	70	700.0	385
10	100h	0.1	80	800.0	440

Table III

Units in μm	**External oxide scale**	**Internal oxide**		**γ′ denuded zone**		**Carbide dissolution**
		Intragranular	**Intergranular**	**Intragranular**	**Intergranular**	
100 hours	0.84 (±0.21)	0.80 (±0.27)	1.55 (±0.26)	1.04 (±0.29)	2.52 (±0.56)	-
2000 hours	1.48 (±0.86)	2.06 (±0.46)	2.92 (±0.48)	2.11 (±0.32)	3.72 (±0.72)	14.50 (±1.81)

Figure 1

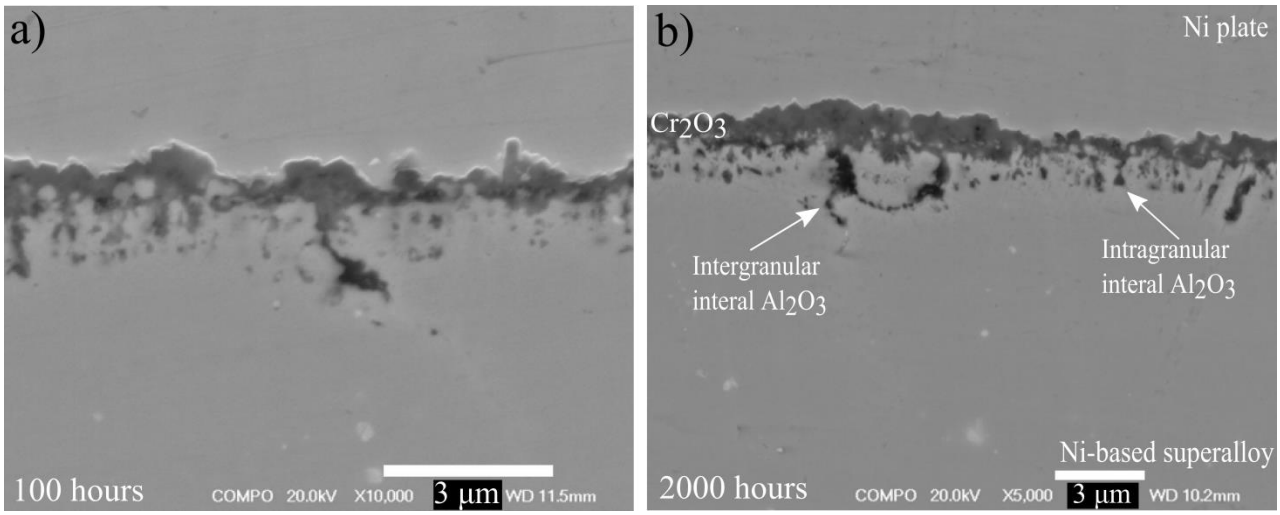
a)
100 hours
COMPO 20.0kV X10,000 3 µm WD 11.5mm
b)
Ni plate
Cr2O3
Intergranular
interal Al2O3
Intragranular
interal Al2O3
Ni-based superalloy
2000 hours
COMPO 20.0kV X5,000 3 µm WD 10.2mm

Figure 2

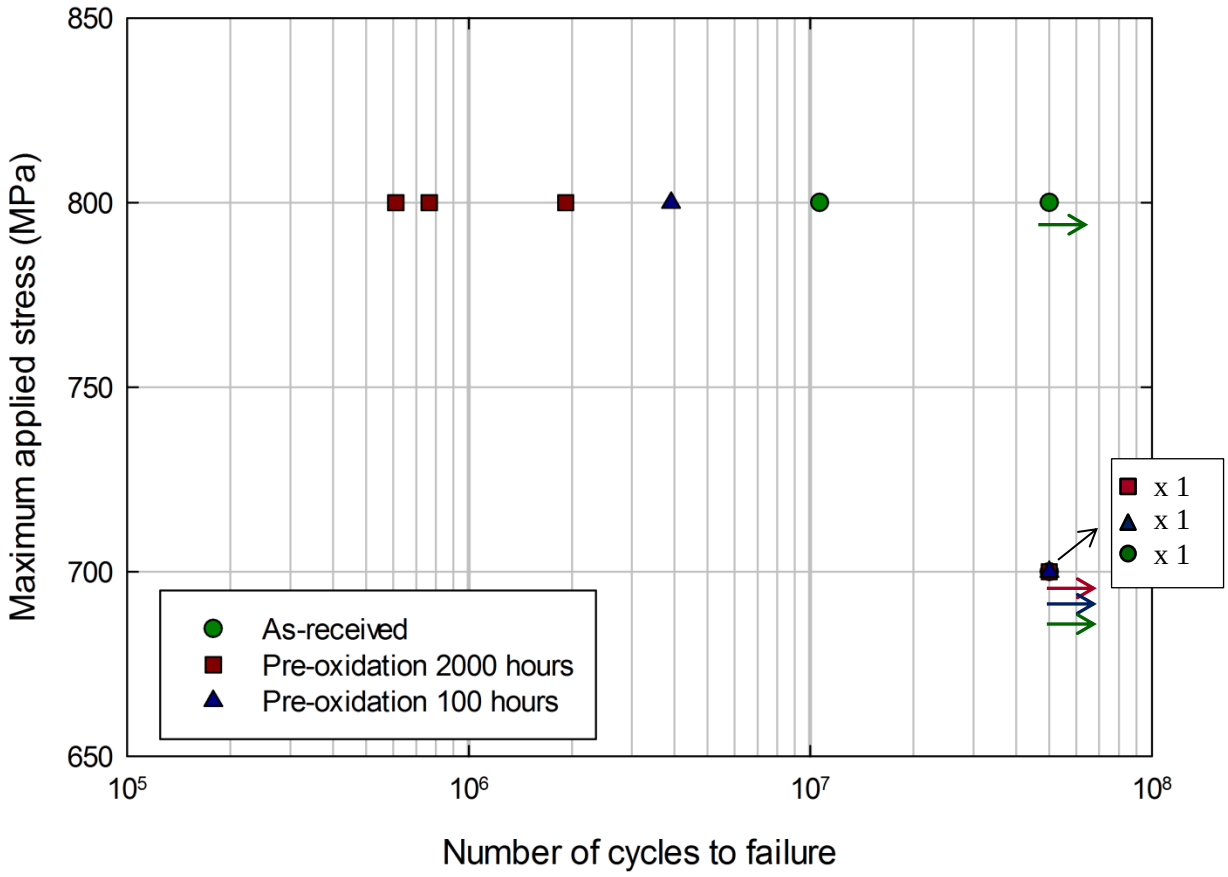
850
800
750
700
650
Maximum applied stress (MPa)
10^5
10^6
10^7
10^8
Number of cycles to failure
As-received
Pre-oxidation 2000 hours
Pre-oxidation 100 hours
x 1
x 1
x 1

Figure 3

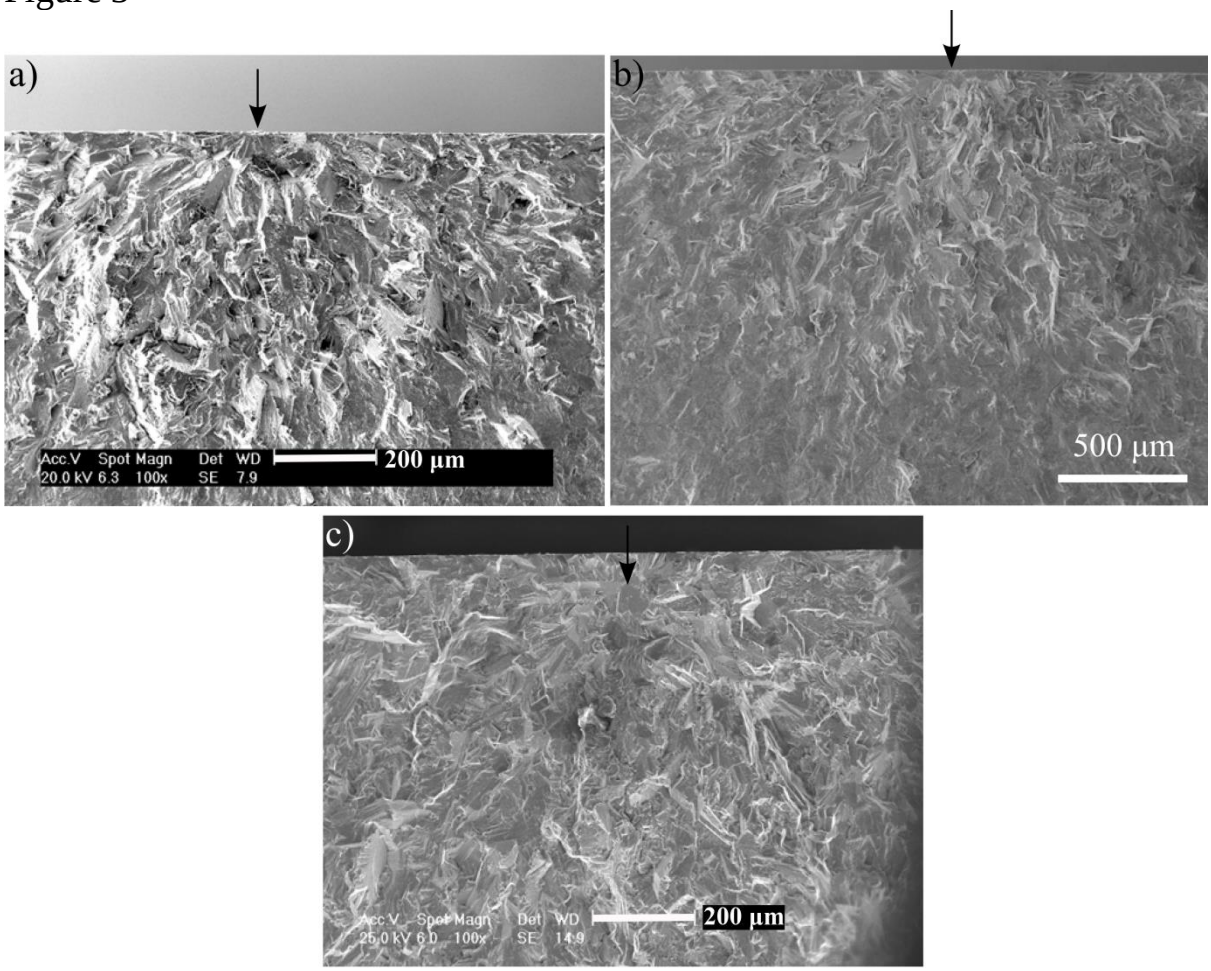
a)
Acc.V Spot Magn Det WD
20.0 kV 6.3 100x SE 7.9
200 µm
b)
500 µm
c)
Acc.V Spot Magn Det WD
25.0 kV 6.0 100x SE 14.9
200 µm

Figure 4

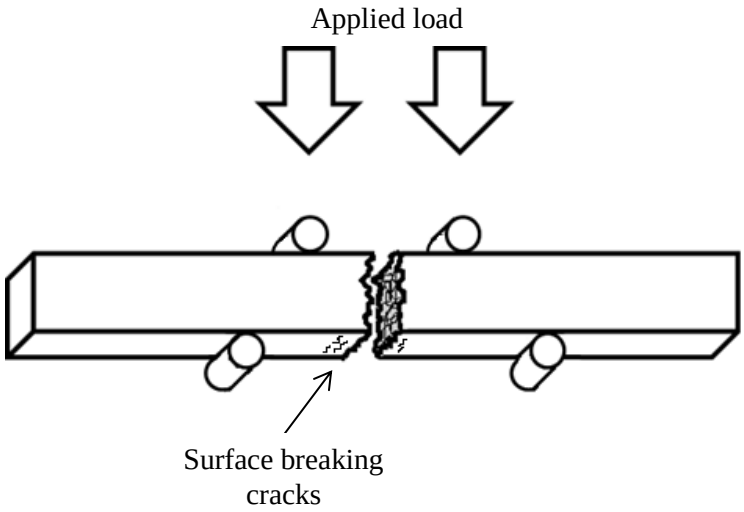

Figure 5

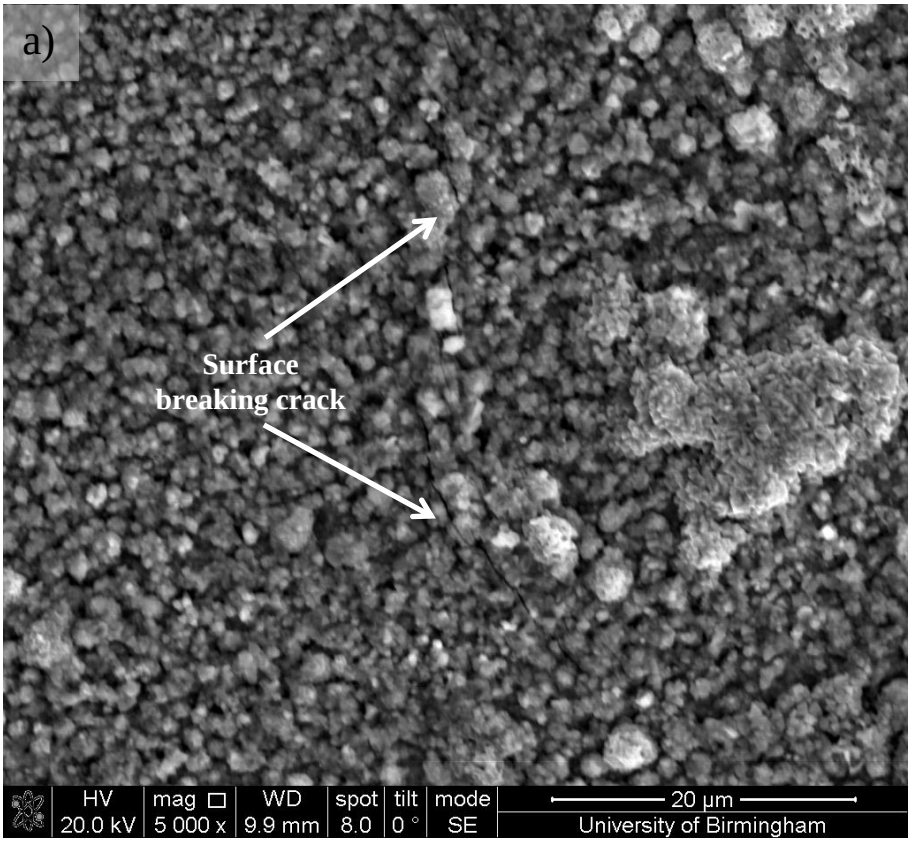
a)
Surface
breaking crack
HV
20.0 kV
mag
5 000 x
WD
9.9 mm
spot
8.0
tilt
0 °
mode
SE
20 µm
University of Birmingham

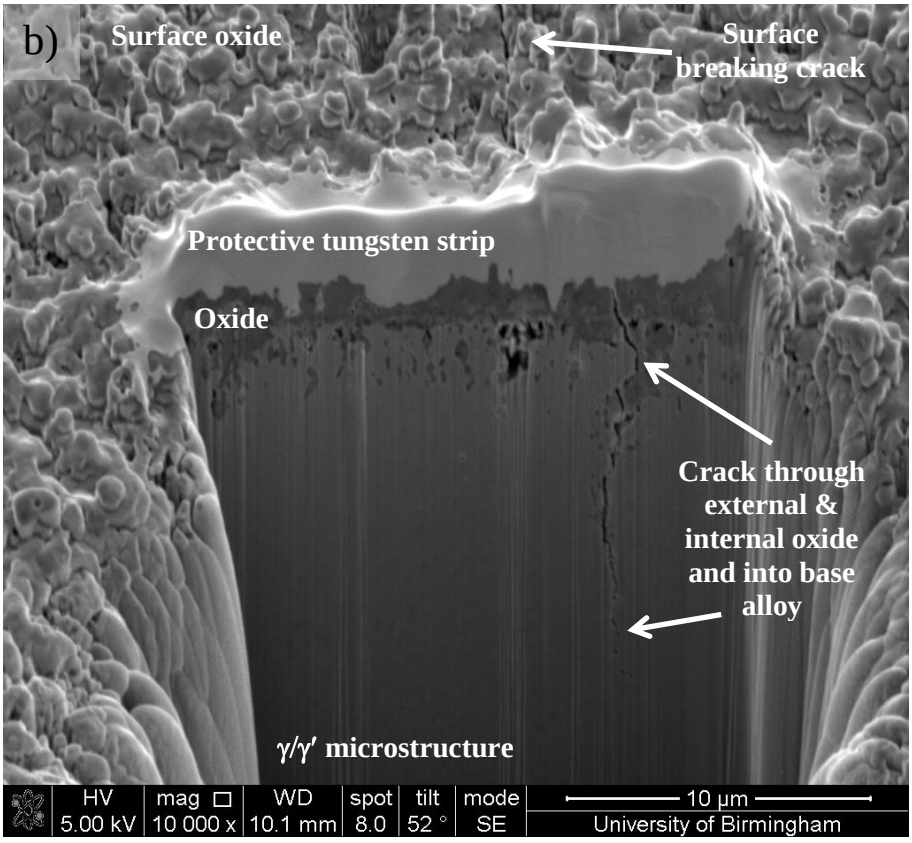
b)
Surface oxide
Surface
breaking crack
Protective tungsten strip
Oxide
Crack through
external &
internal oxide
and into base
alloy
γ/γ′ microstructure
HV
5.00 kV
mag
10 000 x
WD
10.1 mm
spot
8.0
tilt
52 °
mode
SE
10 µm
University of Birmingham

Figure 6

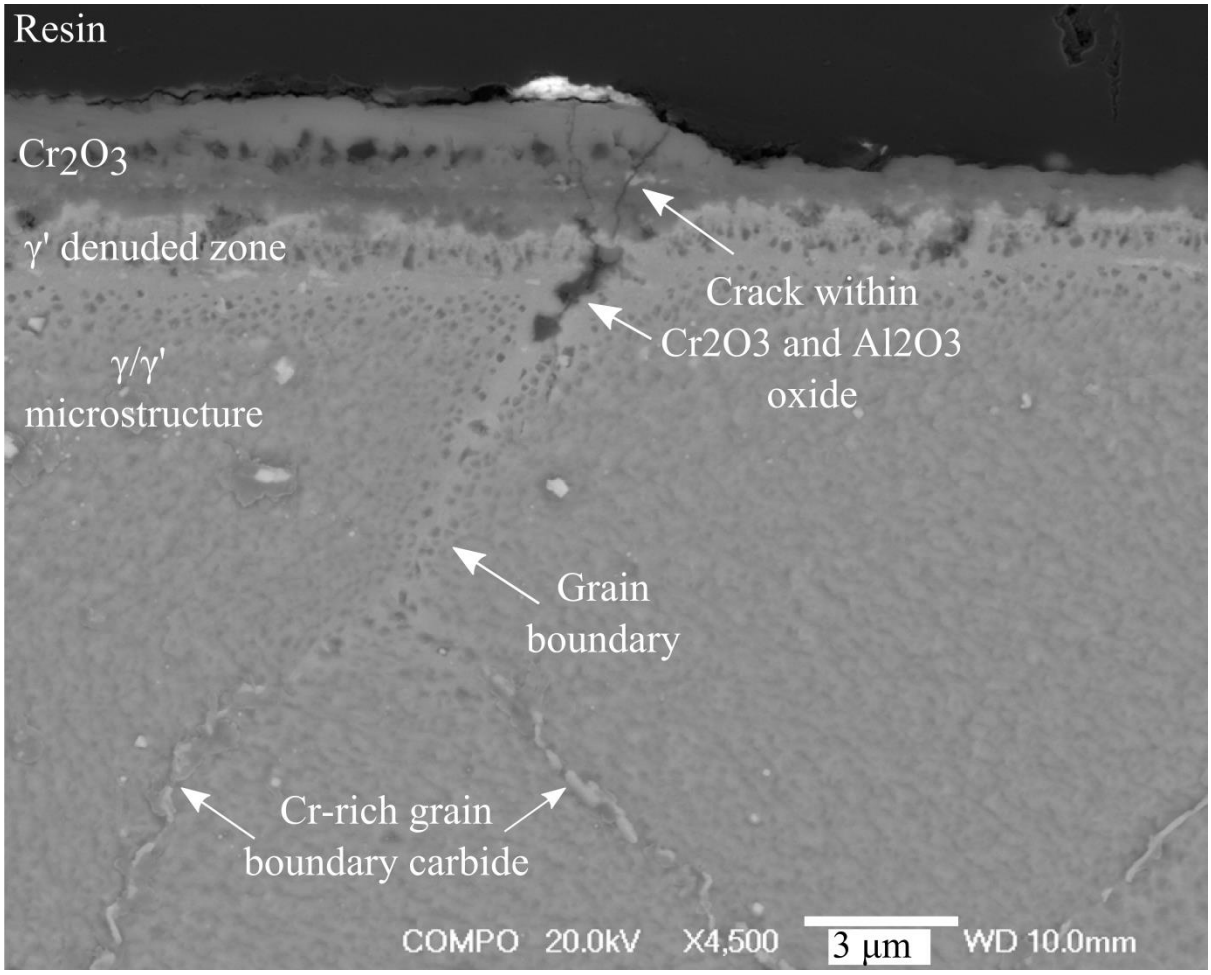
Resin
Cr2O3
γ' denuded zone
γ/γ'
microstructure
Crack within
Cr2O3 and Al2O3
oxide
Grain
boundary
Cr-rich grain
boundary carbide
COMPO 20.0kV X4,500 3 μm WD 10.0mm